High-throughput design of fiber reinforced cement-based composites using deep learning

Zheng Tong [a,b], Jinyang Huo [a], Zhenjun Wang [a,*]

[a] *Chang'an University, School of Materials Science and Engineering, Xi'an, 710061, PR China*
[b] *Sorbonne Université, Université de Technologie de Compiègne, CNRS, UMR 7253 Heudiasyc, CS 60319-60203, Compiègne cedex, France*

ARTICLE INFO

ABSTRACT

As the combinatorial space of a composite is virtually infinite and cannot be explored completely, a deep-learning method was proposed for high-throughput fiber-reinforced cement-based composites (FRC) design. First, a deep hierarchy network was developed to measure the relationship between the experimental variables and the FRC properties. A gradient-based high-throughput method based on the deep hierarchy network was then proposed to design FRCs, which were expected to have one or more certain properties. At last, a fine-tuning method was employed to guarantee its transferability for all types of FRCs. The results showed that the proposed method was able to design cement-fiber-water-curing-aging systems for carbon fiber reinforced cement-based composites (CFRCs). The fine-tuning method could transfer the CFRC model to design other FRCs. Thus, the proposed method showed promise for releasing the composite material property optimization from labor-consuming and low-efficiency laboratory tests.

1. Introduction

In the last two decades, when cement-based composite frameworks (CCFs) emerged as a versatile class of materials for a variety of applications [1,2], the composition and application of CCFs have been the subject of a large body of research [3,4]. A CCF is described by the concept of mixing materials composed of various inorganic, metallic, or/and polymeric materials assembled on cement hydration products. The scientific excitement about CCFs originates in the fact that CCFs can be tuned for a given application by modifying the composed materials, such as material types and contents. Therefore, in principle, the number of possible CCFs is infinitely large; however, since combination and optimization of these materials are time-consuming and laborious [5,6], only a fraction of them have ever been mixed.

Our understanding of CCFs has remained too limited to guide the assembly and combination of these materials. Even the known CCFs are typically not easy to design in practice since diverse and numerous combination methods have existed. This has prevented researchers from drawing a general route for these CCFs. For example, the combinations and design parameters for a CCF, such as fiber-reinforced cement-based

composite (FRC), include fiber types and sizes, fiber distribution, interface interaction zones, temperatures and curing conditions, mixing methods, etc. Considering each parameter as a variable, one needs to probe the high-dimensional combination space constructed by these variables to find a set of the optimal mixture condition leading to the formation of the desirable CCF. Even with abundant prior knowledge, one has to envision a brute force approach, called the large grid search of the combination space (e.g. Refs. [7,8]). The cost of this approach increases exponentially with the number of variables, e.g., testing only three choices for a space of ten variables requires a million experiments. With such poor statistics, a problem arises, how to design a desirable CCF. Further, one may wonder how many CCFs could be composited.

Interestingly, the fact that a large number of CCFs have been developed indicates that researchers can beat brute force statistics by orders of magnitude. More precisely, the researchers' selection of experimental conditions must have been positively biased by their experimental intuition that CCFs have acquired. In this study, the experimental intuition is defined as the collection of unwritten guide-lines used to find the right conditions for CCFs or other composites. It can also be regarded as high-throughput experimentation, which allows
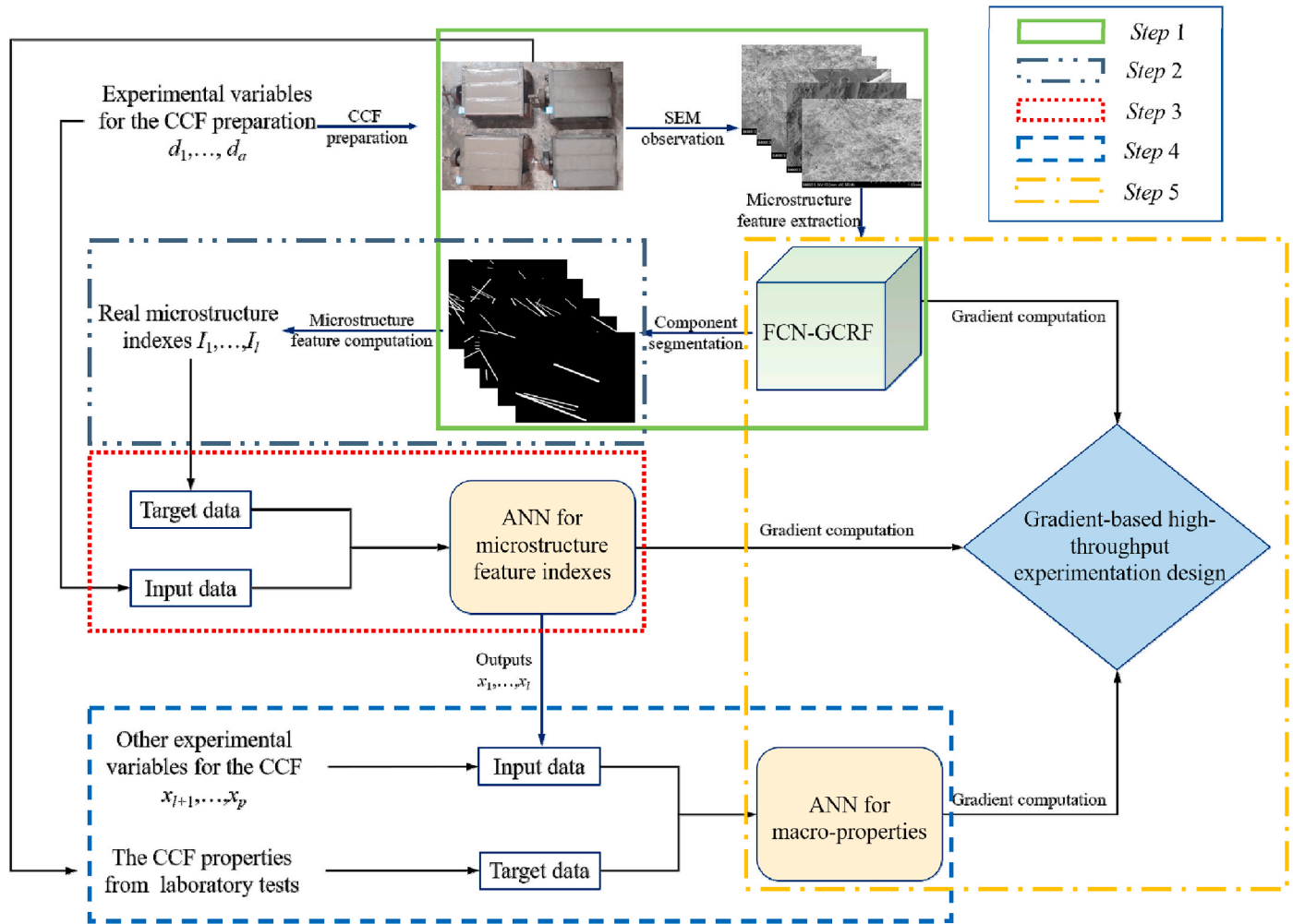

Fig. 1. Workflow of a deep hierarchy network.

the execution of large numbers of experiments to be conducted in parallel while requiring less effort per experiment [9]. Thus, it is critical to capture the experimental intuition for the low-consuming and high-precision CCF design.

There are two main directions for capturing the experimental intuition. One direction is empirical guidelines: empirical equations are developed to build the relationships between the design parameters and the CCFs' properties (e.g. Ref. [10,11]). For example, Xu and Li [12] developed thermal energy storage CCF by incorporating paraffin/diatomite composite phase change material. The quantified relationships among paraffin/diatomite composite, drying shrinkage, and thermal conductivity were measured, which were an original experimental intuition. Zhu et al. [13] proposed the empirical guidelines for the mixing amounts of graphene oxide in the GO CCFs to improve the compressive strength and the flexural strength. Shih et al. [14] measured the effects of nanosilica on the properties of CCFs, and the results showed that a CCF with 0.60% of added nanosilica had an optimum compressive strength. However, these predictions are generally extrapolative in practice [15]. Moreover, the determination of empirical constants is not easy to obtain [16]. Another direction is data-driven guidelines, which captures the experimental intuition from successful CCF experiments results. It is maybe the most promising one and the focus of this paper. Recently, machine learning, as a subset of data-driven methods, has achieved some successes. For example, Wang et al. [17] trained a neural network using an existing database to capture an experimental guideline for the cement mortar with thermo-sensitive poly N-isopropyl acrylamide gels. The experiment results indicated the network predicted the cracking resistance of the modified cement mortar without experiments. Tong et al. [18,19] proposed a deep-learning model to characterize the relationship between fiber distribution and CCFs' properties. This was a data-driven guideline for improving the strength and conductivity of carbon fiber reinforced cement-based composites (CFRCs). Sakthivel et al. [20] used neural networks to capture the experimental intuition of CCFs, which considered specimen sizes, cylinder compressive strength, steel mesh ultimate tensile strength, and mesh volume of reinforcement. Similar works can also be found in Refs. [21–23]. Although some successful cases have been reported in these publications, there are still three problems remaining. The first is that some design parameters of CCFs are not represented reasonably. For instance, the distribution of the mixing materials is a key experimental variable for any CCF. Almost studies use some indirect indexes to characterize the distribution (e.g., fiber mass [24,25], electrical resistance [26], microwave heating uniformity [27]). These indexes cannot characterize the real dispersion morphology of the mixing materials in CCFs, which leads the non-negligible errors in the prediction of CCFs' properties [28]. In fact, Tong et al. [18,19] indicated that the CCFs with the same fiber mass content had different mechanical and electrical properties owing to their various microstructure. Another problem is that only successful CCF conditions have been reported in publications (e.g. Ref. [29,30]), while a substantial amount of time and effort is spent in failed conditions during any research. In practice, the experimental intuition is built from all experiments, such as some failed experiments. A database without failed conditions for machine learning to capture the experimental intuition can be considered as an unbalance learning set, which always leads the low precision [31,32], even makes some ridiculous results. The third is that the transferability and generalization of these data-driven guidelines are limited. It means a guideline for CFRC [33,34] is not suitable for a new CCF [35–38], and accordingly, this has prevented researchers from drawing a general route for these CCFs.

Motivated by these problems, in this work, a deep-learning method was proposed for the high-precision CCF design. We started with developing a deep hierarchy network to measure the relationship between microstructure features and FRC properties, as well as capture the experimental intuition between the experimental variables and the CCF micro-properties. The deep hierarchy network was trained using all of

the successful and failed experiments to capture the generalizable experimental intuition. By analyzing the generated parameters in the deep hierarchy network, a gradient-based high-throughput method was then proposed to design new FRCs, which were expected to have a or more certain properties. Later, a fine-tuning method was employed to guarantee its transferability for all types of FRCs. The contributions of this work, especially the quantified intuition in CCFs, are summarized as follows.

(1) The quantified intuition provided a way to design expected CCFs, which released researchers from the time-consuming and laborious experiments.
(2) The quantified intuition for a CCF was able to be transferred into other CCFs using a few existing successful and failed experiment conditions.
(3) The proposed method had the capacity of designing a cement-fiber-water-preparing-curing-aging system for CCFs with one or more expected properties. The property errors between the predicted and measured values were satisfactory because of the utilization of deep hierarchy networks for characterizing some real microstructure features of CCFs.

The rest of this paper is organized as follows. The proposed methodology is first established in Section 2. The experimental details of this work are described in Section 3, and the results are presented and discussed in Section 4. Finally, the conclusions are summarized in Section 5 of the paper.

2. Methodology

The proposed gradient-based deep learning for capturing the experimental intuition consisted of three parts: a deep hierarchy network, a gradient-based computation, and a fine-tuning method. A deep hierarchy network is first introduced in Section 2.1 to measure the relationship between microstructure features and FRC properties, as well as capturing the experimental intuition between the experimental variables and the CCF macro-properties. The gradient-based method for the FRC design is then described in Section 2.2, followed by a fine-tuning method for guaranteeing the methodology generalization for all FRCs in Section 2.3.

2.1. Deep hierarchy network

Deep hierarchy networks in Ref. [18,19] used scanning electron microscope (SEM) images or other data to characterize the microstructure of CCFs, such as fiber distribution. The networks were then also used to build the relationship among the microstructure features, the experimental variables, and the CCF macro-properties quantitatively. The main advantage of this model was that it represented the microstructure features based on its real morphology rather than some indirect indexes. In this section, the deep hierarchy network is recalled. For a complete introduction, readers are invited to refer to Tong's original work [18,19].

The workflow of a deep hierarchy network is shown in Fig. 1. The deep hierarchy network can be divided into three parts: a feature extractor and two relationship describers. A fully convolutional network (FCN) or its variants was adopted as a feature extractor to extract the microstructure features of CCFs from SEM images or other data. Neural networks or other supervised algorithms, whose input data were the extracted features from SEM images and other direct design variables of CCFs, were used as the relationship describers to build the relationship between the input data and macro-properties of CCFs. In the view of machine learning, the deep hierarchy network was regarded as a deep-learning algorithm as it extracted high-level features from the raw data by combining low-level features [39]. The works of a deep hierarchy network can be summarized in five steps as follows.
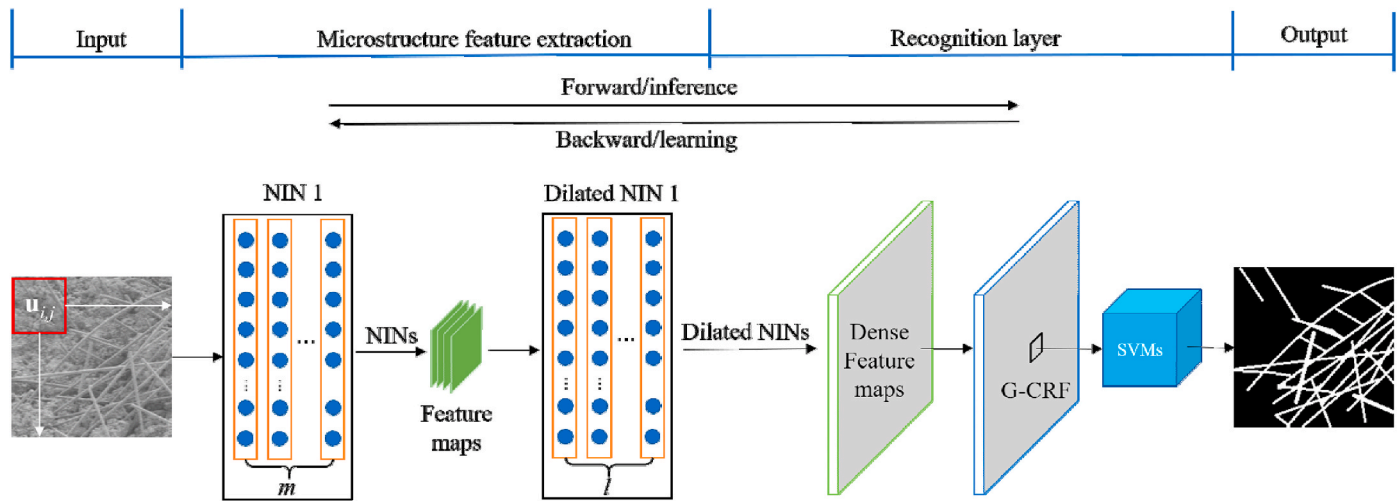
Fig. 2. Architecture of an FCN-GCRF.

Step 1 Give a set of a sample $\mathbf{s} = \{s_1, \ldots, s_n\}$, $s_i \in R^3$ as the data containing the microstructure feature information of a CCF. As some studies [40,41] indicated that SEM images characterized the CCF microstructure precisely, they were used as the data for the microstructure representation, such as fiber distribution and interface interaction. In this study, a novel variant of FCNs was proposed to extract the features as Fig. 2, called the FCN integrated with a Gaussian-conditional random field (FCN-GCRF). Compared to an FCN, the FCN-GCRF provided more desirable results in object segmentation [42,43], which improved the effectiveness of the micro-structure and micro-property evaluation in Step 2. The three main structure layers in an FCN-GCRF can be summarized by the following equations,

$$f_{i,j,k}^1 = ReLU\left(\mathbf{w}_{k,conv}^1 \cdot \mathbf{u}_{i,j} + b_{k,conv}^1\right) \cdots k = 1, \ldots, c \tag{1a}$$

$$f_{i,j,k}^m = ReLU\left(\mathbf{w}_{k,conv}^m \cdot \mathbf{f}_{i,j}^{m-1} + b_{k,conv}^1\right) \cdots k = 1, \ldots, c \tag{1b}$$

$$D_{i,j,p}^1 = ReLU\left(\mathbf{w}_{p,Tconv}^1 \cdot \mathbf{f}_{i,j}^m + b_{p,Tconv}^1\right) \cdots p = 1, \ldots, t \tag{2a}$$

$$D_{i,j,p}^l = ReLU\left(\mathbf{w}_{p,Tconv}^l \cdot \mathbf{D}_{i,j}^{l-1} + b_{p,conv}^1\right) \cdots p = 1, \ldots, t \tag{2b}$$

$$\mathbf{E}\left(\mathbf{D}_{i,j}^l\right) = \frac{1}{2}\left(\mathbf{D}_{i,j}^l\right)^T (A + \lambda\mathbf{I})\mathbf{D}_{i,j}^l - B\mathbf{D}_{i,j}^l \tag{3a}$$

$$\begin{cases} \mathbf{w}_{SVM}^T \mathbf{E}\left(\mathbf{D}_{i,j}^l\right) + b_{SVM} \leq 0, y_{i,j} = +1 \\ \mathbf{w}_{SVM}^T \mathbf{E}\left(\mathbf{D}_{i,j}^l\right) + b_{SVM} \succ 0, y_{i,j} = -1 \end{cases} \tag{3b}$$

where the procedures of a network-in-network (NIN) layer, dilated NIN layer, and recognition layer are described as Eq. (1), Eq. (2), and Eq. (3), respectively. First, as shown in Eq. (1), network-in-network (NIN) layers are used to approximate the representation of the latent concepts related to the microstructure by element-by-element multiplications, multiplied value addition, bias addition, and ReLU activation. The fundamental structure of a NIN layer can be found in the study of Lin et al. [44]. In Eq. (1), m is the sub-layer number in a NIN layer. Matrix $u_{i,j}$, called receptive filed of size $i \times j \times o$, is a patch of a input data with the size of $\left(\frac{W-i+2p}{r} + 1\right) \times \left(\frac{W-i+2p}{r} + 1\right) \times o$. Notably, o in the first NIN layer shown in Fig. 2 is 3, the same as the channel of SEM images. A NIN layer with an r stride and a p padding can generate a $W \times H \times c$ tensor, called feature maps. The size of a feature map is $W \times H \times 1$, while the channel number of the feature maps is c. The activated outputs in each sub-layer number of a NIN layer are $\mathbf{f}_{i,j}^l = (f_{i,j,1}^l, \ldots, f_{i,j,c}^l)$, $l = 1, \ldots, m$. Second, as shown in Eq. (2), dilated network-in-network layers are used to upsample, in which the feature maps generated by the final NIN is dilated to the same size as the input SEM image, while the extracted microstructure features are remained. A dilated NIN layer, regarded as a variation of a NIN layer with dilated convolution operations [45], has the same work principle as a NIN layer. Finally, as shown in Eq. (3), the dilated feature maps are transferred by a Gaussian random field, and each pixel in the dense feature maps is classified into one of the components in a CCF by SVMs to conduct the pixel-level segmentation. In Eq. (3a), A and B are a symmetric $N \times N$ matrix of pairwise terms and an $N \times 1$ vector of unary terms, respectively. $N = \left(\frac{W-i+2p}{r} + 1\right) \times \left(\frac{H-i+2p}{r} + 1\right)$. Therefore, $\mathbf{E}(\mathbf{D}_{i,j}^l)$ can be considered as the posterior log-likelihood of the inferred hypothesis $\mathbf{D}_{i,j}^l$, which represents the relationships between pixels in the outputs. In Eq. (3b), w_{svm} and b_{svm} are weights and biases of a SVM; $y_{i,j}$ is the class that a pixel belongs to. An example of step 1 is shown in Fig. 2. Different components in a SEM image are segmented by the FCN-GCRF to represent the microstructure features of a CCF.

Step 2: Compute the real microstructure indexes $I_1, \ldots, I_l$ using the

segmentation results of the FCN-GCRF. For example, Tong's original work [18] presented as a real fiber distribution index as

$$D_{SEM} = \frac{A_{Singlefiber}}{A_{Nofiber} + A_{fibercluster} + A_{Singlefiber}} \tag{4a}$$

$$D_{sample} = \frac{1}{n}\sum_{i=1}^n D_{SEM,i}, \tag{4b}$$

where D_{sample} and D_{SEM} were the fiber distribution in the CCF and the observation area of a SEM image, respectively. $A_{No\ fiber}$, $A_{Single\ fiber}$, and $A_{fiber\ cluster}$ were the areas of background, single fibers and fiber clusters, respectively. The pixel areas of single fibers and fiber clusters were the fiber and cluster areas in the observation area of a SEM image, while the rests in the SEM image were considered as the area of background. Similarly, other microstructure indexes were also proposed, such as real interface interaction areas IIA as

$$IIA = \frac{1}{n}\sum_{i=1}^n \frac{A_{interactionarea,i}}{A_{interactionarea,i} + A_{background,i}}. \tag{5}$$

Step 3 Build the relationship between the design variables for the CCF preparation $d_1, \ldots, d_a$ and microstructure feature indexes $I_1, \ldots, I_l$ using an artificial neural network (ANN), as shown in the red box in Fig. 1. Step 3 is described as

$$mic_{i_1}^1 = \tanh\left(\sum_{j=1}^a w_{i_1,j}^1 d_j + b_{i_1}^1\right) \cdots i_1 = 1, \ldots, a_{pre}^1 \tag{6a}$$

$$mic_{i_2}^2 = \tanh\left(\sum_{j=1}^{i_1} w_{i_2,j}^2 mic_j^1 + b_{i_2}^2\right) \cdots i_2 = 1, \ldots, a_{pre}^2 \tag{6b}$$

$$mic_{i_v}^v = \tanh\left(\sum_{j=1}^{i_{v-1}} w_{i_v,j}^v mic_j^{v-1} + b_{i_v}^v\right) \cdots i_v = 1, \ldots, a_{pre}^v \tag{6c}$$

where, v is the layer number in an ANN; a_{pre}^b (b = 1, …,v) is the neuron number in each layer, and $w_{i_c,j}^c$ and $b_{i_c}^c$ (c = 1, …,v) are weights and biases in the ANN, respectively. The final outputs are $\mathbf{mic}^v = (mic_1^v, \ldots mic_{a_{pre}^v}^v) = (x_1, \ldots, x_l)$, and $a_{pre}^v = l$.

Step 4 Define a pattern $\mathbf{x} = \{x_1, \ldots, x_l, \ldots, x_p\}$ including the extracted features from SEM images and other direct experimental variables of CCFs as shown in the blue box in Fig. 1, and predict the macro-properties of a CCF with design parameters $\mathbf{x}$ as

$$pro_{\gamma_1}^1 = \tanh\left(\sum_{j=1}^p \alpha_{\gamma_1,j}^1 x_j + \beta_{\gamma_1}^1\right) \cdots \gamma_1 = 1, \ldots, a_{pro}^1 \tag{7a}$$

$$pro_{\gamma_2}^2 = \tanh\left(\sum_{j=1}^{a_{pro}^1} \alpha_{\gamma_2,j}^2 pro_j^1 + \beta_{\gamma_2}^2\right) \cdots \gamma_2 = 1, \ldots, a_{pro}^2 \tag{7b}$$

$$pro_{\gamma_\delta}^\delta = \tanh\left(\sum_{j=1}^{a_{pro}^{\delta-1}} \alpha_{\gamma_\delta,j}^\delta pro_j^{\delta-1} + \beta_{\gamma_\delta}^\delta\right) \cdots \gamma_\delta = 1, \ldots, a_{pro}^\delta \tag{7c}$$

where (p-l) is the number of other direct experimental variables of CCFs, δ is the layer number in the ANN, a_{pro}^d (d = 1, …,δ) is the neuron number in each layer, and $\alpha_{\gamma_e,j}^e$ and $\beta_{\gamma_e}^e$ (e = 1, …,v) are weights and biases in the ANN. The final outputs are $\mathbf{pro}^\delta = (pro_1^\delta, \ldots pro_{a_{pro}^\delta}^\delta)$, and its dimension is the expected property number of the CCF.

Step 5 The weights in the deep hierarchy network were used to analyze the relationship among the experimental variables, the microstructure features, and the macro-properties of CCFs [19]. In this study, a gradient-based method was proposed not only to analyze the relationship but also to conduct the high-precision CCF design, which will be

introduced in Section 2.2.

In this study, we designed several FCN-GCRFs with different numbers of NIN and dilated NIN layers to find the optimal architecture. The FCN-GCRF with the minimum loss in the validation set was considered optimal. Users can also directly refer to the original works about FCN-GCRF [42,43] to design one if they just need a desirable one. The strategy to find the optimal ANNs in Step 3 and Step 4 is the same as those in FCN-GCRFs.

2.2. Gradient-based computation

Give an learning set $\chi = \{(\mathbf{x}^1,\mathbf{y}^1), …, (\mathbf{x}^n,\mathbf{y}^n)\}$, in which $\mathbf{x}^i=(x^i_1, …,x^i_l, …,x^i_p)$, $i = 1, …,n$, is a set of the experimental variables in CCFs, and $\mathbf{y}^i = (y^i_1, …y^i_{a^{\delta}_{pro}})$ is the corresponding CCF properties measured by laboratory tests. Using χ, weights and bias in Eq. (1) ~ Eq. (7) are adjusted by a backpropagation algorithm [46]. In the backpropagation algorithm, the gradients of the weights and the bias are used for the adjustment to reduce the error between the predicted properties $\mathbf{pro}^{\delta}(\mathbf{x}^i) = (pro^{\delta}_1(x^i), …, pro^{\delta}_{a^{\delta}_{pro}}(x^i))$ and the measured testing properties $\mathbf{y}^i = (y^i_1, …y^i_{a^{\delta}_{pro}})$. In this study, a similar gradient-based method was proposed to adjust a set of experimental variables $\mathbf{x} = \{x_1, …,x_l, …,x_p\}$ for designing a CCF, which was expected to have certain properties $\mathbf{pro}^{\delta}(\mathbf{x})$ ($pro^{\delta}_1(x)$, …$pro^{\delta}_{a^{\delta}_{pro}}(x)$). The method can be summarized as following:

Step 1 Select representative patterns $\mathbf{p}^1, …,\mathbf{p}^{\varepsilon}$ from the existing learning set χ. $\mathbf{p}^i=(\mathbf{x}^i_{\mathbf{pi}},\mathbf{rp}^i)$, $i = 1, …,\varepsilon$. Then a loss between each representative pattern $\mathbf{p}^i$ and $\mathbf{pro}^{\delta}(\mathbf{x})$ is computed as

$$Loss(\boldsymbol{p}^i,\boldsymbol{x}) = \left\| \boldsymbol{y}^{p^i} - \mathbf{pro}^{\delta}(\boldsymbol{x}^i) \right\|^2_2 \quad, i=1,…,\varepsilon. \tag{8}$$

Step 2 The gradients w.r.t. $x_1, …,x_l, …,x_p$ in Eq. (8) are computed as

$$\frac{\partial Loss(\boldsymbol{p}^i,\boldsymbol{x})}{\partial pro^{\delta}_{\gamma_{\delta}}(\boldsymbol{x})} = 2(pro^{\delta}_{\gamma_{\delta}}(\boldsymbol{x}) - rp^i_{\gamma_{\delta}})\gamma_{\delta} = 1,…,a^{\delta}_{pro} \tag{9a}$$

$$\frac{\partial Loss(\boldsymbol{p}^i,\boldsymbol{x})}{\partial pro^{\delta-1}_{\gamma_{\delta-1}}(\boldsymbol{x})} = \sum_{\gamma_{\delta}=1}^{a^{\delta}_{pro}} \frac{\partial Loss(\boldsymbol{p}^i,\boldsymbol{x})}{\partial pro^{\delta}_{\gamma_{\delta}}(\boldsymbol{x})} \cdot \left(1 - pro^{\delta}_{\gamma_{\delta}}(\boldsymbol{x})^2\right) \cdot \alpha^{\delta}_{\gamma_{\delta},\gamma_{\delta-1}} \cdots \gamma_{\delta-1} = 1,…,a^{\delta-1}_{pro} \tag{9b}$$

$$\frac{\partial Loss(\boldsymbol{p}^i,\boldsymbol{x})}{\partial pro^1_{\gamma_1}(\boldsymbol{x})} = \sum_{\gamma_2=1}^{a^2_{pro}} \frac{\partial Loss(\boldsymbol{p}^i,\boldsymbol{x})}{\partial pro^2_{\gamma_2}(\boldsymbol{x})} \cdot \left(1 - pro^2_{\gamma_2}(\boldsymbol{x})^2\right) \cdot \alpha^2_{\gamma_2,\gamma_1} \cdots \gamma_1 = 1,…,a^1_{pro} \tag{9c}$$

$$\frac{\partial Loss(\boldsymbol{p}^i,\boldsymbol{x})}{\partial x_j} = \sum_{\gamma_1=1}^{a^1_{pro}} \frac{\partial Loss(\boldsymbol{p}^i,\boldsymbol{x})}{\partial pro^1_{\gamma_1}(\boldsymbol{x})} \cdot \left(1 - pro^1_{\gamma_1}(\boldsymbol{x})^2\right) \cdot \alpha^{\delta}_{\gamma_1,j} \cdots j = 1,…,l,…,p \tag{9d}$$

As $x_{l+1}, …,x_p$ are the direct experimental variables of CCFs, their gradients can be directly used in the next step. However, $x_1, …, x_l$ are the indirect experimental variables generated by the ANN for microstructure feature indexes, as shown in Fig. 1. Thus, the gradients w.r.t. the experimental variables for the CCF preparation $d_1, …,d_a$ are computed as

$$\frac{\partial Loss(\boldsymbol{p}^i,\boldsymbol{x})}{\partial mic^{v-1}_{i_{v-1}}(\boldsymbol{x})} = \sum_{i_v=1}^{a^p_{pre}} \frac{\partial Loss(\boldsymbol{p}^i,\boldsymbol{x})}{\partial x_j} \cdot \left(1 - x_j^2\right) \cdot w^v_{i_v,i_{v-1}} \cdots i_{v-1} = 1,…,a^{v-1}_{pre} \tag{10a}$$

$$\frac{\partial Loss(\boldsymbol{p}^i,\boldsymbol{x})}{\partial mic^1_{i_1}(\boldsymbol{x})} = \sum_{i_2=1}^{a^1_{pre}} \frac{\partial Loss(\boldsymbol{p}^i,\boldsymbol{x})}{\partial mic^2_{i_2}(\boldsymbol{x})} \cdot \left(1 - mic^2_{i_2}(\boldsymbol{x})^2\right) \cdot w^2_{i_2,i_1} \cdots i_1 = 1,…,a^1_{pre} \tag{10b}$$

$$\frac{\partial Loss(\boldsymbol{p}^i,\boldsymbol{x})}{\partial d_j} = \sum_{i_1=1}^{a^1_{pre}} \frac{\partial Loss(\boldsymbol{p}^i,\boldsymbol{x})}{\partial mic^1_{i_1}(\boldsymbol{x})} \cdot \left(1 - mic^1_{i_1}(\boldsymbol{x})^2\right) \cdot w^1_{i_1,j} \cdots j = 1,…,a \tag{11c}$$

where $\partial Loss(\boldsymbol{p}^i,\boldsymbol{x}) \big/ \partial mic^v_{i_v}(\boldsymbol{x}) = \partial Loss(\boldsymbol{p}^i,\boldsymbol{x}) \big/ \partial x_j$.

Step 3 The experimental variables $d_j(\mathbf{p}^i)$ and $x_j(\mathbf{p}^i)$ associated to $\mathbf{p}^i$ is defined as following:

$$d_j(\boldsymbol{p}^i) = d^i_{\boldsymbol{pi},j} - \frac{\partial Loss(\boldsymbol{p}^i,\boldsymbol{x})}{\partial d_j} \cdots j = 1,…,a \tag{12a}$$

$$x_j(\boldsymbol{p}^i) = x^i_{\boldsymbol{pi},j} - \frac{\partial Loss(\boldsymbol{p}^i,\boldsymbol{x})}{\partial x_j} \cdots j = l+1,…,p \tag{12b}$$

where $d^i_{\boldsymbol{pi},j} = (d^i_{\boldsymbol{pi},1}, …, d^i_{\boldsymbol{pi},a})$ and $x^i_{\boldsymbol{pi},j} = (x^i_{\boldsymbol{pi},l+1}, …, x^i_{\boldsymbol{pi},p})$ are the experimental variables associated to $\mathbf{p}^i$.

Step 4 The final design parameters $d_1, …,d_a$ and $x_{l+1}, …,x_p$ can be computed based on each $d_j(\mathbf{p}^i)$ and $x_j(\mathbf{p}^i)$ as

$$d_j = \sum_{i=1}^{\varepsilon} k^i \cdot d_j(\boldsymbol{p}^i) \cdots j = 1,…,a \tag{13a}$$

$$x_j = \sum_{i=1}^{\varepsilon} k^i \cdot x_j(\boldsymbol{p}^i) \cdots j = l+1,…,p \tag{13b}$$

$$k^i = \frac{1}{Loss(\boldsymbol{p}^i,\boldsymbol{x}) \cdot \sum_{m=1}^{\varepsilon} Loss(\boldsymbol{p}^m,\boldsymbol{x})}, \cdots i = 1,…,\varepsilon \tag{13c}$$

2.3. Fine-tuning method

By learning the existing experiments in a type of CCFs, researchers can capture the experimental intuition and transfer it to another CCFs. For example, one who can determine the experimental parameters of CFRCs also can learn how to design an SFRC. The gradient-based method in Section 2.2 provided a way to capture the experimental intuition of one type of CCFs. The transferability of the method was required to improve its generalization. A fine-tuning approach was proposed by referring to Ref. [47,48]. Generally, transferring learning can be divided into two directions: feature transferring and model transferring. In the proposed approach, the two directions are used as follows:

(1) As the microstructure features of CFRCs and other CCFs are similar, the feature transferring was utilized to fine-tune the FCN-GCRF in a deep hierarchy network. Give a database of the SEM images of SFRCs $\mathbf{s'} = \{s'_1, …,s'_m\}$, in which m is less than the number of the SEM images for CFRC. The weights in the NIN and dilated layers of the FCN-GCRF for CFRCs do not need to be updated by $\mathbf{s'}$. We can directly use the NIN and dilated layers to extract the features from $\mathbf{s'}$, in which the outputs are the dense feature maps, as shown in Fig. 2. Then, w_{svm} and b_{svm} in each SVM of the FCN-GCRF are fine-tuned based on the dense feature maps with a small learning rate. In this study, the learning rate was 1×10^{-5}. Finally, the FCN-GCRF for SFRC consists of the NIN layers, the dilated layers, and the updated SVMs.

(2) The two ANNs in the deep hierarchy network are used to capture the experimental intuition based on the microstructure features and other experimental variables. Model transferring is used to fine-tune the two. Give a learning set $\chi' = \{(\mathbf{x'}^1,\mathbf{y'}^1), …, (\mathbf{x'}^q, \mathbf{y'}^q)\}$, in which q is much less than the data number for CFRC. The weights and bias in the two ANNs are fine-tuned by χ' with a backpropagation algorithm using a small learning rate [46]. In this study, the learning rate was 1×10^{-5}.
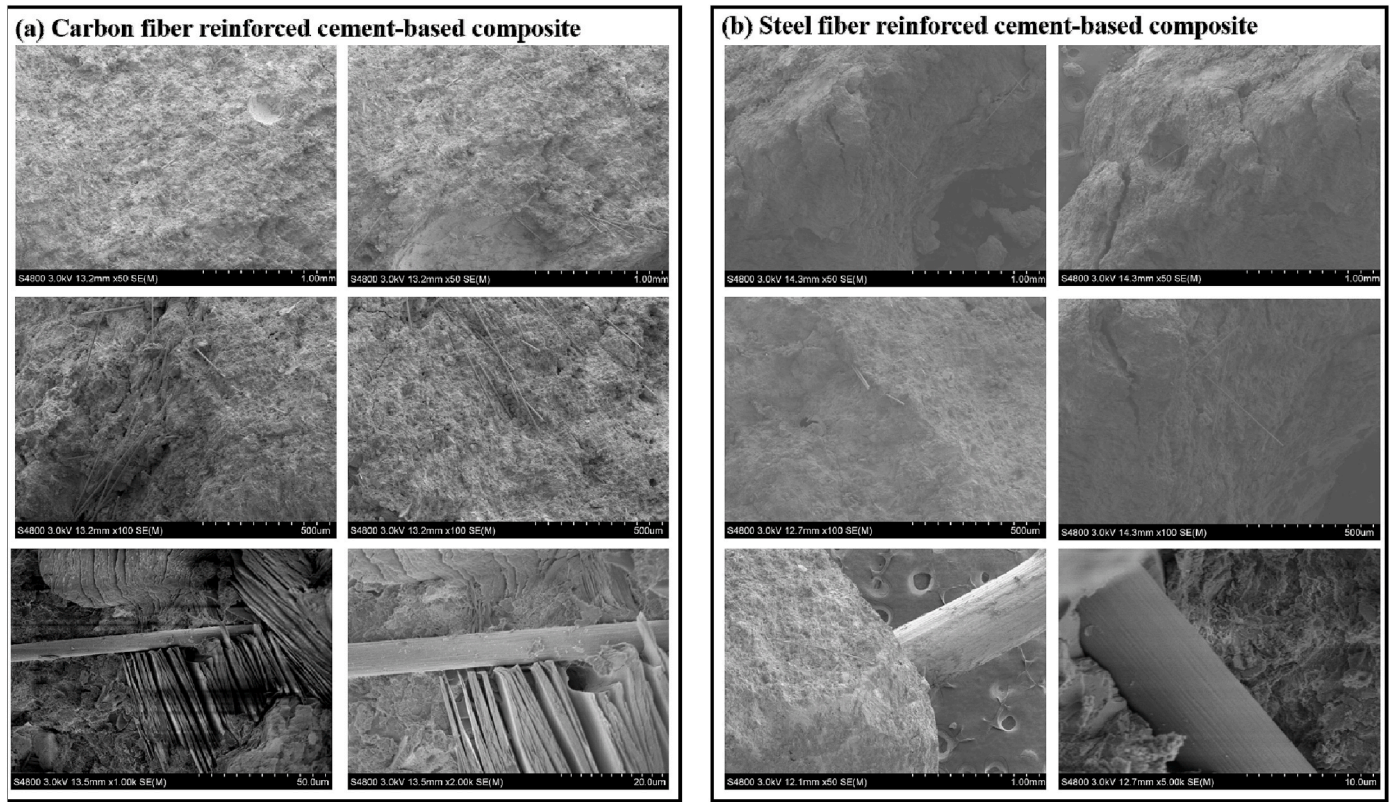
Fig. 3. SEM images of FRC.

3. Experimental details

3.1. Experiment database

As introduced in Section 2, three databases are required to develop a deep hierarchy network and capture the experimental intuition to design CFRCs as follows.

(1) The database for the microstructure features extraction. The database in our previous study was still used in this study, whose availability has been fully discussed in Ref. [18]. The database was made up of 7597 SEM images with three magnifications (× 50, × 100, and × 200). There were 4557 training images, 1520 validation images, and 1520 testing images. Some examples are

shown in Fig. 3(a). These SEM images were used as the input data for the FCN-GCRF, whose outputs were the segmented components in these SEM images, as shown in Fig. 2.

(2) The database to train and validate the ANN for microstructure feature indexes. In our previous works [18,19,28,49], only some of successful experiments was reported. In this study, the successful and failed experiment results were all used to capture the experimental intuition. Totally, 674 experiment results were collected, in which the ratio between the successful and failed experiment results were approximately 1:2.40. There were 406 training samples, 134 validation samples, and 134 testing samples. The ratios between the successful and failed samples in the training, validation, and testing samples were all about 1:2.40.

(3) The database to train and validate the ANN for macro-properties design had the same size as the database to train and validate the ANN for microstructure feature indexes.

Similarity, three databases were used to conduct the experimental intuition transfer as follows:

(1) The database for the microstructure features extraction. The database was made up of 526 SEM images for SFRC with three magnifications (× 50, × 100, and × 200). There were 316 training images, 105 validation images, and 105 testing images. Some examples are shown in Fig. 3(b).

(2) The database to train and validate the ANN for microstructure feature indexes. The database consisted of 62 training samples, 20 validation samples, and 20 testing samples. The ratio between the successful and failed experiment results was approximately 1:2.10.

(3) The database to train and validate the ANN for macro-properties design had the same size as the database to train and validate the ANN for microstructure feature indexes.
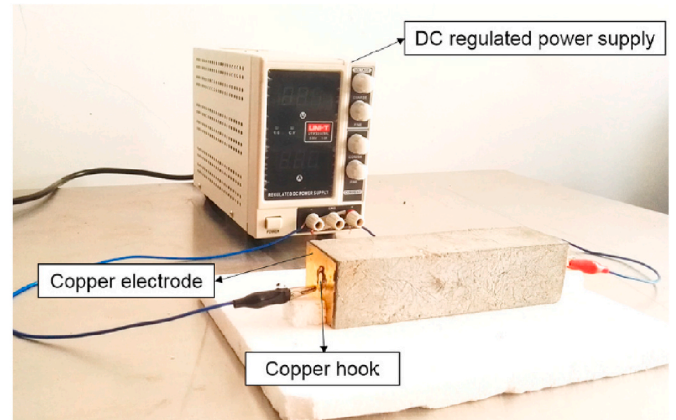
Table 1
Testing experiments.

No.	CCF type	Bending strength /MPa	Electrical conductivity/(Ω·m)	Thermal conductivity/ (W/(m·K))
Test 1	CFRC	12.0	50.0	–
Test 2	CFRC	15.0	–	–
Test 3	CFRC	7.0	–	2.50
Test 4	CFRC	8.5	100.0	2.00
Test 5	SFRC	7.5	30.0	3.00
Test 6	SFRC	7.0	100.0	–
Test 7	SFRC	8.0	–	–
Test 8	SFRC	8.0	–	2.70

(a) Bending strength

(b) Electrical conductivity

(c) Thermal conductivity

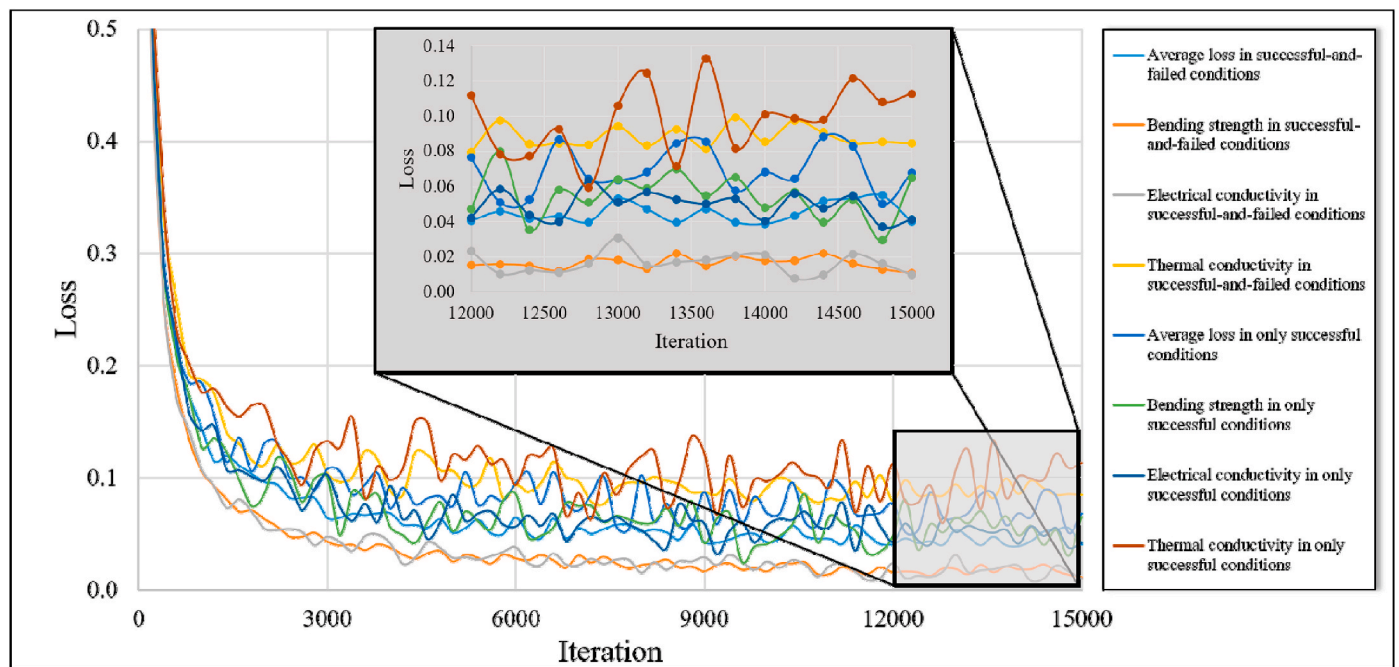**Fig. 4.** Setups for macro-property measurement.

Fig. 5. Validation performance of deep hierarchy networks in the two training conditions.

Table 2
FCN- GCRF architecture.

Layer	Input data	Sub-layers	Output data	Stride
Input	$226 \times 226 \times 3$	–	–	–
NIN 1	$226 \times 226 \times 3$	$9 \times 3 \times 1$	$224 \times 224 \times 96$	1
NIN 2	$224 \times 224 \times 96$	4×1	$112 \times 112 \times 96$	1
NIN 3	$112 \times 112 \times 96$	$25 \times 18 \times 6 \times 1$	$54 \times 54 \times 256$	2
NIN 4	$54 \times 54 \times 256$	$25 \times 18 \times 6 \times 1$	$25 \times 25 \times 384$	2
NIN 5	$25 \times 25 \times 384$	$25 \times 18 \times 6 \times 1$	$10 \times 10 \times 384$	2
NIN 6	$10 \times 10 \times 384$	$4 \times 2 \times 1$	$4 \times 4 \times 768$	2
NIN 7	$4 \times 4 \times 768$	$4 \times 2 \times 1$	$2 \times 2 \times 4096$	2
NIN 8	$2 \times 2 \times 4096$	4×1	$1 \times 1 \times 1000$	1
Dilated NIN 1	$1 \times 1 \times 1000$	1×4	$2 \times 2 \times 4096$	1
Dilated NIN 2	$2 \times 2 \times 4096$	$1 \times 2 \times 4$	$4 \times 4 \times 768$	2
Dilated NIN 3	$4 \times 4 \times 768$	$1 \times 2 \times 4$	$10 \times 10 \times 384$	2
Dilated NIN 4	$10 \times 10 \times 384$	$1 \times 6 \times 18 \times 25$	$25 \times 25 \times 384$	2
Dilated NIN 5	$25 \times 25 \times 384$	$1 \times 6 \times 18 \times 25$	$54 \times 54 \times 256$	2
Dilated NIN 6	$54 \times 54 \times 256$	$1 \times 6 \times 18 \times 25$	$112 \times 112 \times 96$	2
Dilated NIN 7	$112 \times 112 \times 96$	1×4	$224 \times 224 \times 96$	1
Dilated NIN 8	$224 \times 224 \times 96$	$1 \times 3 \times 9$	$226 \times 226 \times 3$	1
Gaussian random field	$226 \times 226 \times 3$	–	$226 \times 226 \times 3$	–
SVMs	$226 \times 226 \times 3$	–	$226 \times 226 \times 3$	–

Table 3
Architectures of two ANNs.

Layer	ANN for microstructure feature indexes	ANN for macro-properties
Input	fiber mass content, water-cement ratio, mixing method, stirring time, stirring speed, and dispersing agent	fiber distribution, interface interaction areas, curing temperature, curing humidity, curing time, fiber strength, fiber electrical conductivity, fiber thermal conductivity, and cement strength
Hidden	$10 \times 15 \times 5 \times 2$	$15 \times 20 \times 7 \times 3$
Output	fiber distribution and interface interaction areas	bending strength, electrical conductivity, thermal conductivity

In all the databases, there were six experimental variables for CCF preparation (fiber mass content, water-cement ratio, mixing method, stirring time, stirring speed, and dispersing agent), two real microstructure indexes (fiber distribution and interface interaction areas), seven other direct CCF experimental variables (curing temperature and humidity, curing time, fiber strength, fiber electrical conductivity, fiber thermal conductivity, and cement strength), and three expected macro-properties (bending strength, electrical conductivity, thermal conductivity). Notably, the mixing methods and types of dispersing agent were orthogonal coded [50], while other variables were normalized based on the maximum and minimum values in the databases.

3.2. Testing experiment

Eight testing groups were conducted to verify the effectiveness of the proposed method, as shown in Table 1. Table 1 does not present some values of electrical and thermal conductivities because some groups of CCFs are not required to have one or more certain properties. For example, only bending strength and electrical conductivity should be considered when we design a CFRC as a conductive cement composite, such as Test 1.

The method introduced in Section 2 was first used to determine the experimental variables for the eight groups. Then, the CCF groups were prepared and cured, and their properties were measured. The bending strengths were measured using a material testing system, as shown in Fig. 4(a). The loading rate was controlled at 0.05 mm/s. The distance between the loading and each support was 50 mm. The distance between the support and the specimen top was 30 mm. The electrical conductivities were measured by a self-developed setup, as shown in Fig. 4(b) [49]. The thermal conductivities were measured using an infrared camera, as shown in Fig. 4(c). The infrared images were collected after each 30s microwave heating, and the total time was 5 min. The thermal conductivities were calculated by taking the average of the temperature

changes in each pixel.

4. Results and discussion

4.1. Capturing experimental intuition using deep learning

One can safely state that the bodywork on CFRCs, even CCFs, involves thousands of experiments, of which only the successful conditions have been published. In this discussion, we started by providing the difference in capturing the experimental intuition between the only successful conditions and the successful-and-failed conditions. The validation performance of the deep hierarchy networks trained in the two conditions is shown in Fig. 5. The architectures of the FCN-GCRF and the two ANNs are shown in Table 2 and Table 3, which were determined by the validation loss after training, as mentioned in Section 2.1. The final losses of the two models using Eq. (8) were 0.04 and 0.06, respectively. The losses demonstrated that the two deep hierarchy networks predicted the CFRC macro-properties (bending strength, electrical conductivity, and thermal conductivity) with a 4% and 6% average error once given a set of the experimental parameters from the validation data set. As the validation data set introduced in Section 3.1 included a large number of the combination and conditions for preparing CFRC, the generalization of the two networks were acceptable, but the one capturing experimental intuition from successful-and-failed conditions was better. McNemar's test, as a statistical test for paired nominal data, was also conducted to compare the predictive accuracy of the two networks. In this work, p-value in the McNemar's test was computed as

$$p = 2 \sum_{i=b}^{b+c} \binom{n}{i} . 0.5^i (1 - 0.5)^{b+c-i} \qquad (14)$$

where b was the number of the training samples predicted correctly by the deep hierarchy network trained in the successful-and-failed conditions but predicted incorrectly by the deep hierarchy network trained in the only successful conditions; c was the number of the training samples predicted incorrectly by the deep hierarchy network trained in the successful-and-failed conditions but predicted correctly by the deep hierarchy network trained in the only successful conditions. For complete information about McNemar's test, readers are invited to read the original work of McNemar [52]. In this work, a sample was considered to be predicted correctly when its average gap between the predicted and measured macro-properties was less than 5%. The p-value of the deep hierarchy networks was 0.013. Thus, the effect of the use of the failed conditions was statistical and significant (p-value<0.05). Thus, the structure of a deep hierarchy network had the capacity to capture the experimental intuition from both successful and failed experiments. Interestingly, the characteristic of the deep hierarchy network was close to those of researchers. The proposed method learned how to prepare a CFRC by a series of failed experiments, the same as a human did.

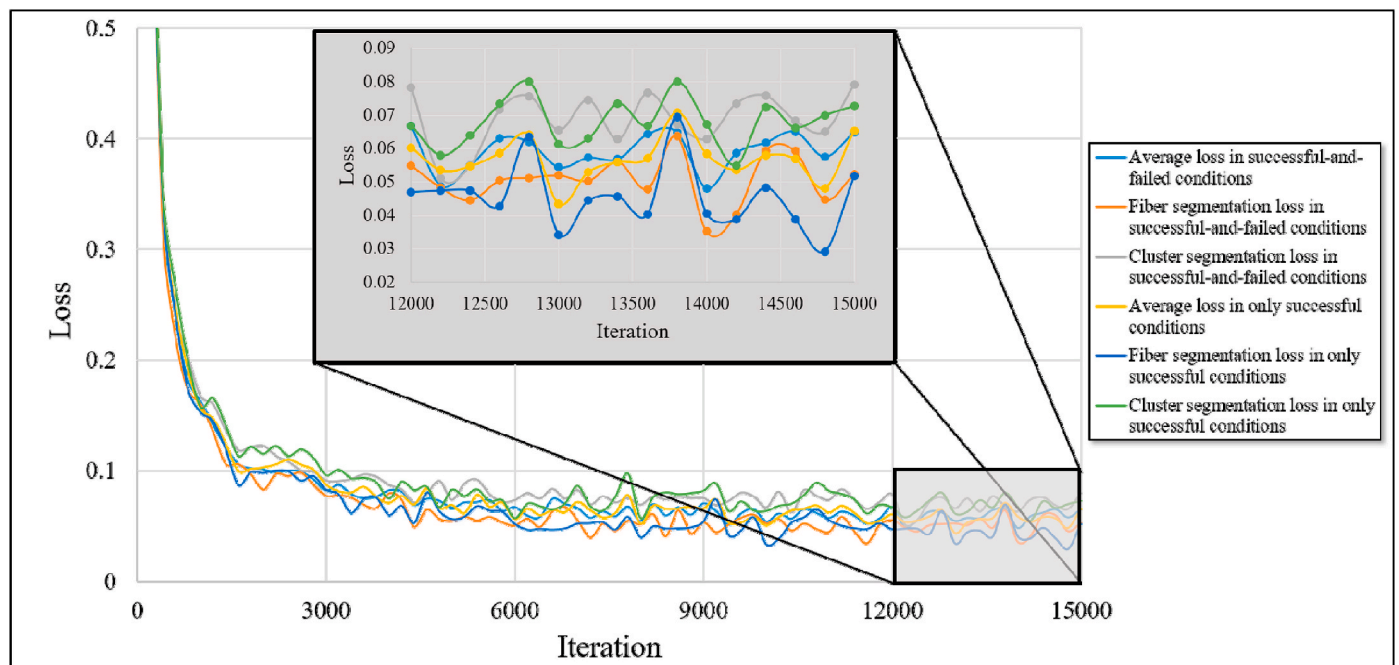Additionally, the final losses of the electrical conductivity were the

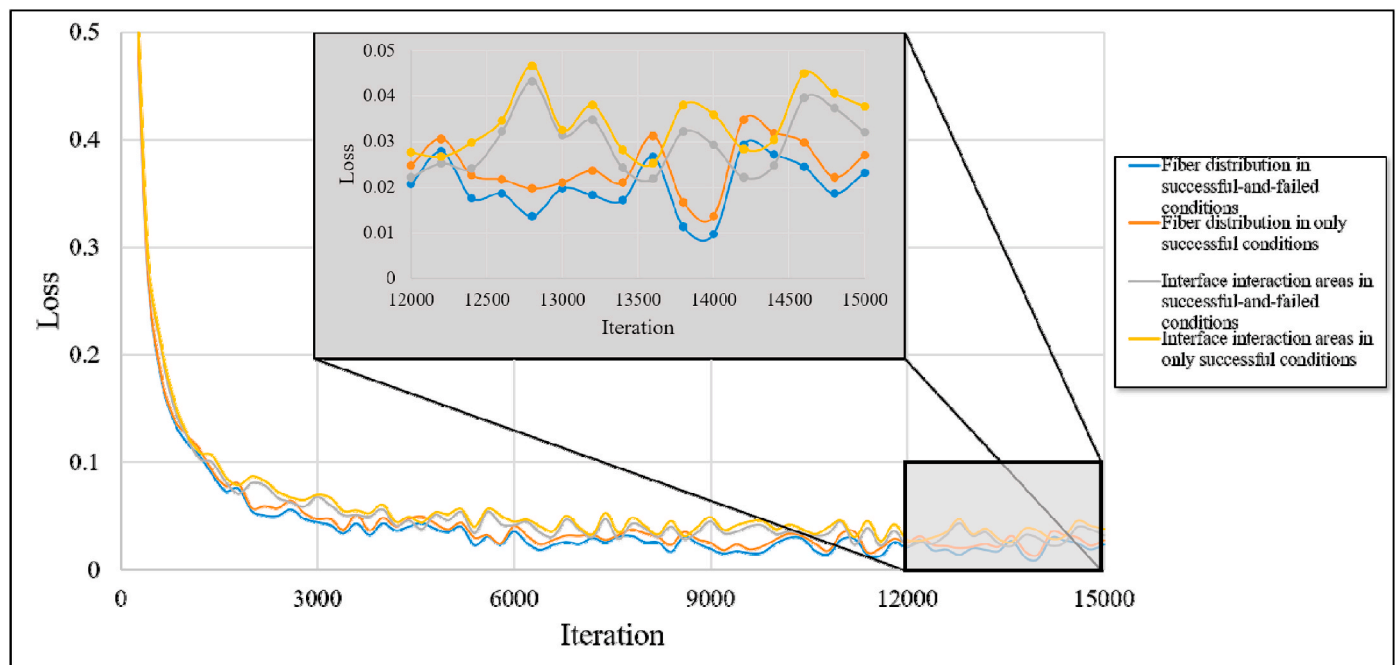**Fig. 6.** Validation performance of the FCN-GCFRs in the two training conditions.

Fig. 7. Validation performance of the ANNs for microstructure feature indexes in the two training conditions.
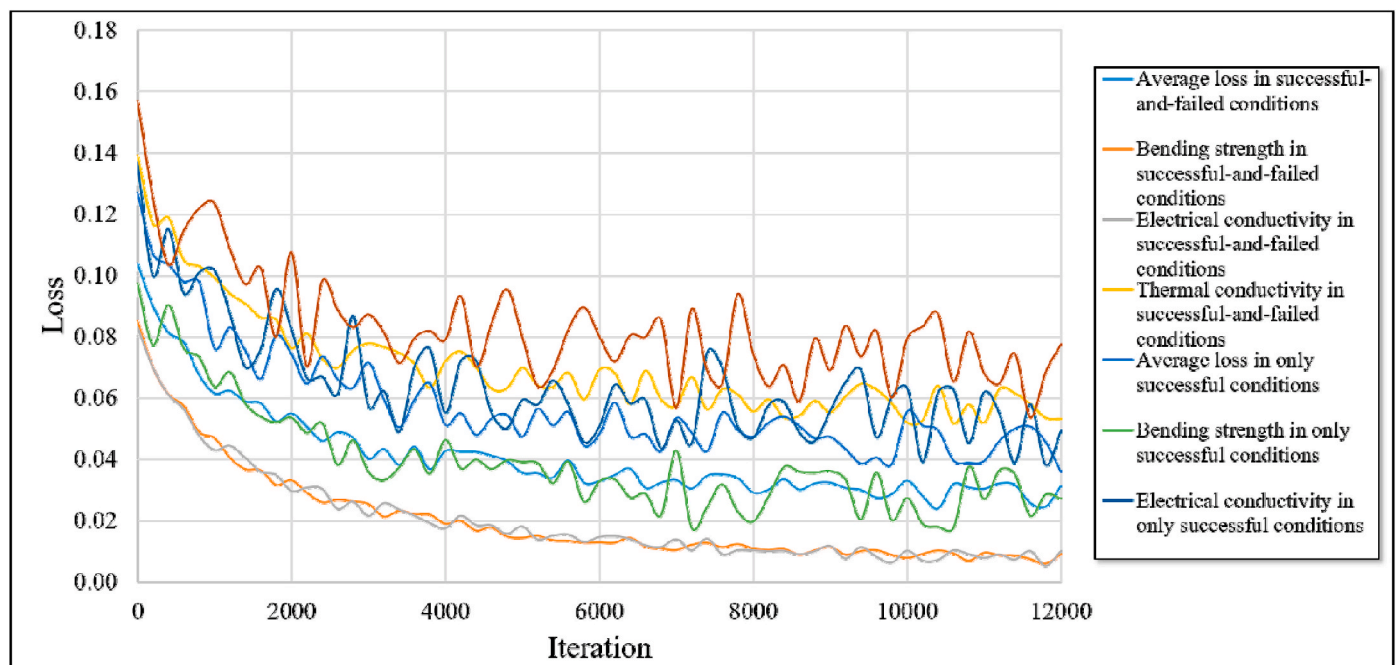
Fig. 8. Validation performance of transferring networks in the two training conditions.

Table 4
Design parameters for the testing experiments.

	Test 1	Test 2	Test 3	Test 4	Test 5	Test 6	Test 7	Test 8
Fiber mass content/%	0.841	1.232	0.327	0.567	0.547	0.214	0.914	1.342
Water-cement ratio/%	0.32	0.35	0.33	0.34	0.36	0.32	0.35	0.35
Mixing method	After-mixing	Before-mixing	After-mixing	After-mixing	After-mixing	After-mixing	Before-mixing	After-mixing
Stirring time/s	161	192	114	142	138	92	172	207
Stirring speed/(r/min)	60	60	60	60	60	60	60	60
Curing temperature/°C	20	19	20	21	22	21	22	20
Curing humidity/%	94	96	92	92	93	93	94	94
Curing time/day	16	26	14	14	16	14	17	17
Fiber strength/MPa	2000–2300	2000–2300	1800–2100	2000–2100	600–700	500–600	600–800	600–800
Fiber electrical conductivity/ $(10^{-3}\Omega$ cm)	0.5-0.7	–	–	0.9-1.0	$(1.45\text{–}1.65) \times 10^{-3}$	$(2.10\text{–}2.40) \times 10^{-3}$	–	–
Fiber thermal conductivity/(W/ (m·K))	–	–	60–80	40–50	45–50	–	–	40–45
Cement flexural strength (28 d)/ MPa	7.5–8.2	7.8–8.3	7.2–8.0	7.3–7.6	7.3–7.5	7.3–7.7	7.3–8.2	7.3–7.9

maximum in the three properties, as well as the loss fluctuations in Fig. 5. This was because the database uncertainty regarding the electrical conductivity was higher than those regarding the other two properties, which led the models to capture less useful features and experimental intuition regarding the electrical conductivity. In the view of CFRC property measurement, the database uncertainty might arise from two reasons: (1) the self-developed setup did not work as well as expected; (2) some experimental variables of CFRC were not considered in this model, but they had the effects on the electrical conductivity. One of the solutions for the database uncertainty was to collect more data. As there were hundreds of reported success CFRC cases in the world, the database uncertainty might be removed by learning the successful and failed results from other groups' experiment results. A similar suggestion was also proposed by Moosavi et al. [51].

The losses of the FCN-GCFRs and ANNs in the two deep hierarchy networks trained in two conditions are shown in Fig. 6 and Fig. 7. The losses of the two FCN-GCFRs were close. The p-value of McNemar's test for the segmentation errors in the two conditions was 0.0007. The same situation can also be found in the ANNs for microstructure feature indexes. This indicated that the failed experiment results were not able to improve the performance of the microstructure feature extraction. Therefore, only the processes for building the relationship between the experimental variables and the macro-properties needed the failed experiment results.

Fig. 8 presents the validation performance of the two transfer networks for SFCR. The final losses of the two transfer models were 0.031 and 0.053, which was close to the losses of the two deep hierarchy networks for CFRC, even though the training samples in SFCR was not as abundant as those in CFRC. Additionally, the initial losses of the two transfer models were from 0.104 to 0.127, which were much less than those of the deep hierarchy networks for CFRC. This was because the experimental intuition captured from the CFRC database has the similarity as those for designing SFRC. Thus, only a fine-tuning method was required to transfer the CFRC experimental intuition to the SFRC experiment intuition using a small database. Similarly, a researcher can quickly learn how to design other CCFs after conducting a small number of experiments if he/she knows the method to design CFRCs. Thus, the procedures of transfer learning for capturing the experiment intuition had some similarity with those of a researcher transferring the knowledge to a similar objective.

4.2. Performance of CCF design

We now illustrate that the quantified experimental intuition has the capacity of designing the CCFs, which have the expected macro-properties. By using the well-trained models in Section 4.1 and the gradient-based computation in Section 2.2, we designed the CCFs with

the properties shown in Table 1.

Table 4 presents the design parameters for the testing experiments shown in Table 1. Fig. 9 shows the expected and real properties of the testing experiments. The errors between the expected and real properties were less than 8.0%, which were close to the testing performance of the network trained in the successful-and-failed conditions. As expected, the proposed method considered the gradients as the quantified experimental intuition and utilized them to design the CCFs. In addition, Table 4 presents that the selection ranges of the raw materials, such as the electrical conductivity of the fiber properties, decreases with the increase in the numbers of the expected properties. This was because these experiment variables jointly affected the macro-properties of CCFs. Thus, it was not easy for a researcher to design a CCF with two or more satisfactory properties because their experimental intuition was qualitative. However, our proposed method captured and quantified the experimental intuition from the existing experiments, which overcame this problem. It also demonstrated that it was economical to allow the proposed method to consider the expected properties and ignore the other properties. With the decrease in the selected ranges, the preparation of the raw materials became difficult, which led to a high cost in the CCF design. The eight groups without some certain properties in Table 1 demonstrated that the proposed method considered the expected properties and ignored the others.

Two other methods for designing CCFs were selected to compare with the proposed one. The first was also a neural network-based method but did not consider the microstructure indexes. In this method, an ANN was developed using the dataset in Section 3.1. The architecture of the ANN was the same as those of the ANN for macro-properties, as shown in Table 3. However, it did not consist of the microstructure-index inputs (fiber distribution and interface interaction areas). The second was a laboratory-based method, in which one tried to find the design parameters by conducting several experiments. As shown in Fig. 9, the proposed method outperformed the neural network-based method. This demonstrated that the use of the microstructure indexes in the gradient-based method improved the efficiency of the CCF design. The average computational costs of the proposed and neural network-based methods to design a testing group were about 65 ms and 60 ms, respectively. Thus, the proposed method introduced little delay during the testing. Additionally, the laboratory-based method could not provide the parameters to design the CCFs whose two or more properties were expected. For example, the electrical and thermal conductivities in Test 1 were different from the expected ones, even though its bending strength was satisfactory.

Fig. 10 presents the gradients of Test 4 w.r.t. representative patterns $\mathbf{p}^1, \ldots, \mathbf{p}^\varepsilon$ from the existing learning set χ. In this study, ε was 10. The gradients of each experimental variable associated with each representative pattern were various, which quantified the relative importance of
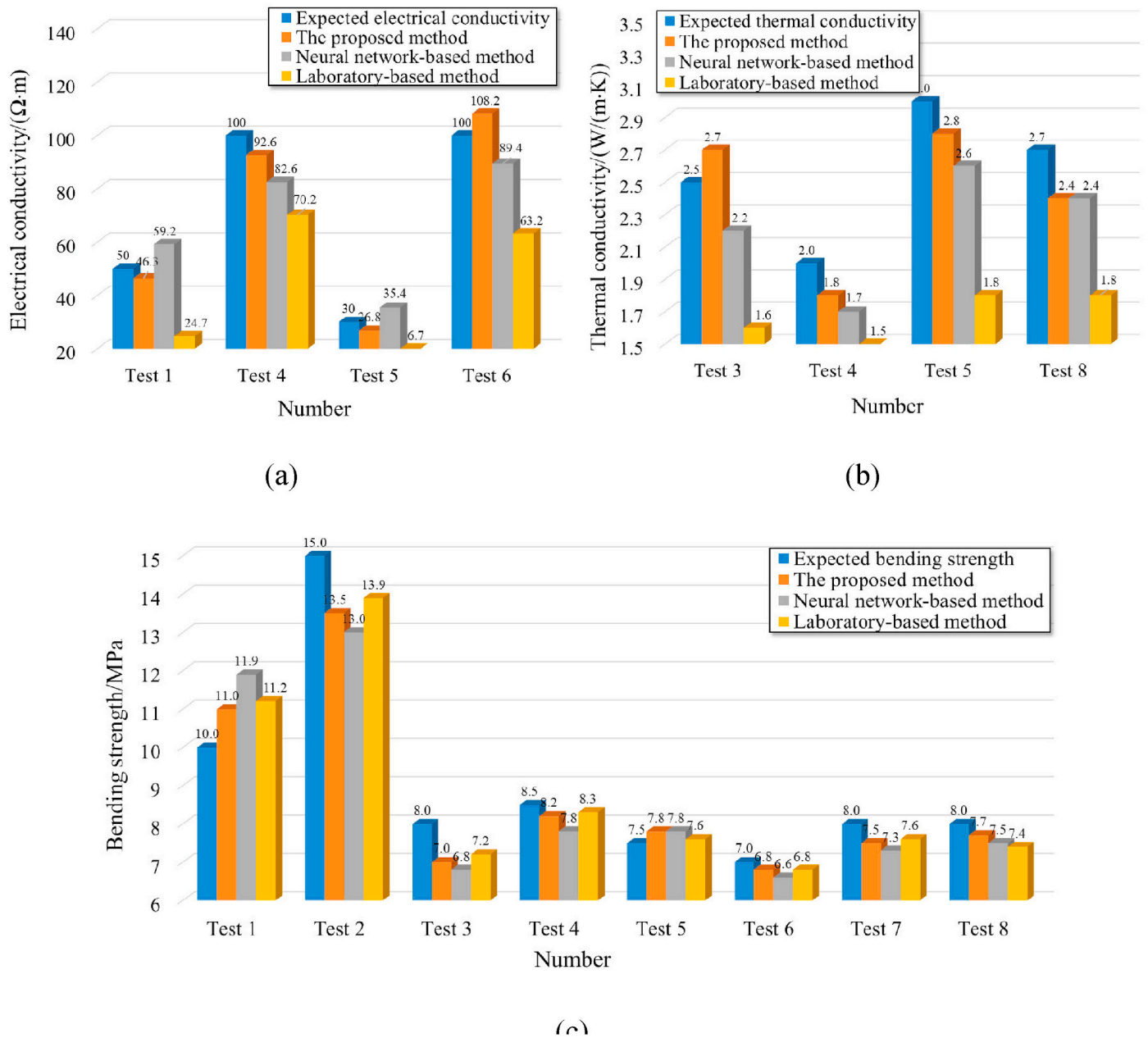
(a)

(b)

(c)

Fig. 9. Expected and real properties of the testing experiments.
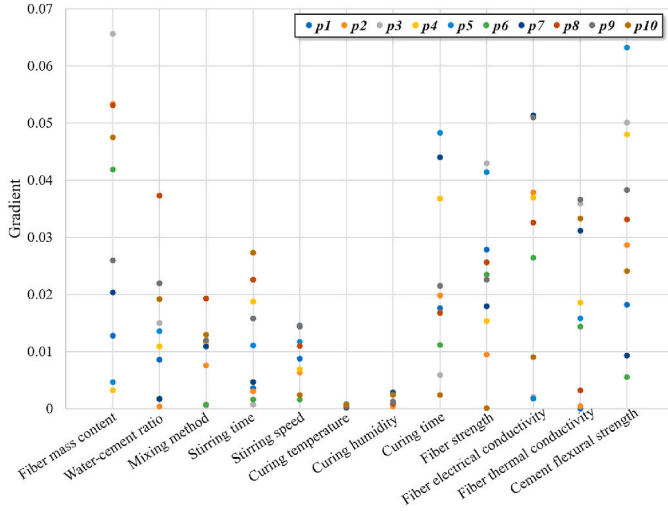
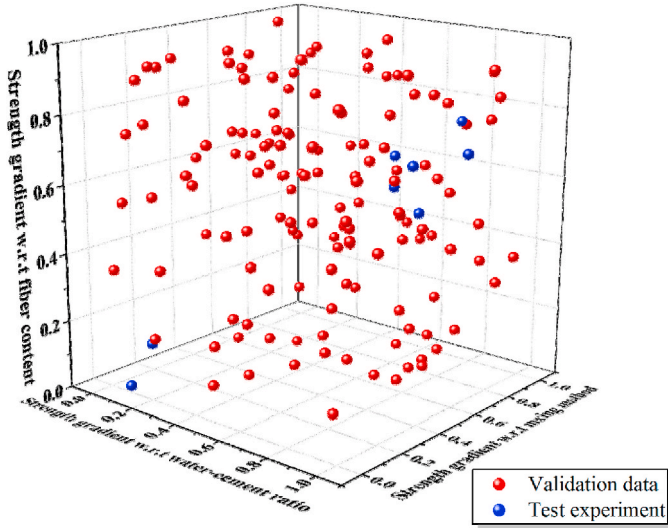**Fig. 10.** Gradients of the first testing experiments w.r.t. representative patterns.

Fig. 11. A visual explanation of the experimental intuition.

Fig. 12. Schematics of the components of the methodology used for CCFs.

The red dots are the validation data set for the ANN for macro-properties design in the deep hierarchy network under the successful-and-failed conditions. As the validation data set was generated before capturing the experimental intuition, it was regarded as the data without prior knowledge. Without prior knowledge, the red dots were uniformly distributed in the gradient space. This indicated that the researchers had no ideas to design a CCF. The blue dots are the data of the testing experiments introduced in Section 3.2. The distribution of the blue dots could be divided into two parts: (a) a space close to the representative patterns $\mathbf{p}^1$, in which the strength results of the testing experiments were close to the strength of $\mathbf{p}^1$; (b) a space far away from the representative patterns $\mathbf{p}^1$, in which the strength results of the testing experiments were different from the strength of $\mathbf{p}^1$. This demonstrated that the use of the gradient-based method as the prior knowledge made it easy to design a CCF with the expected properties, even for someone has little knowledge of CCFs.

4.3. Potential for releasing property optimization from laboratory tests

The main aim of this work is to develop a simple yet powerful methodology that allows one to use failed and successful experiments to improve CCF design strategies systematically. This methodology does not rely on a detailed understanding of how the different experimental variables impact the outcome. Instead, it heavily relies on the notion that, throughout many experiments, researchers develop an intuition on how to approach the problem of finding the optimal design strategies. Here, we have developed a simple way of capturing this experimental intuition using deep learning.

Our case study of CFRC is intended as a proof of principle that we can capture and quantify experimental intuition and effectively use it to develop more CFRC design strategies, even transfer to the SFRC design strategies. Our case was also a proof that the proposed method has the potential for releasing CCF property optimization from time-consuming and laborious laboratory tests. Only a gradient computation and parameter adjustment are required to design a CCF with the expected properties once a researcher has a well-trained deep hierarchy network. Even one can develop their own model if an ideal database is available. Thus, if all groups that have worked on the CCFs would have published their successful experiments as well as failed cases, the data would be significantly less homogenous because of other influencing variables. The much larger data set would also make it easier for deep learning to

the design parameters on the CCFs. For example, the normalized gradients of the first and fourth design parameters (fiber content and stirring time) w.r.t. $\mathbf{p}^1$ were 0.0128 and 0.0036. The strength of the representative pattern $\mathbf{p}^1$ and Test 4 were 14.4 MPa and 8.5 MPa, respectively. The fiber content and stirring time of the representative pattern $\mathbf{p}^1$ were 0.800% and 160 s. The fiber content and stirring time of Test 4 were 0.567% and 142, as shown in Table 2. The fiber contents made more contributions than stirring time to the strength in the range of 8.5–13.4 MPa. Therefore, the normalized gradients of the experimental variables w.r.t the representative pattern provided a novel way to measure the contributions of different experimental variables to the macro-properties. In practice, a researcher, who have done the $\mathbf{p}^1$ experiment, will typically capture the experimental intuition and prefer to adjust the fiber content rather than the stirring time to prepare a CFRC with an 8.5 MPa bending strength. The gradient-based method based on the recorded data allowed us to quantify this intuition and utilize it for subsequent experiments.

Fig. 11 shows a visual explanation of the experimental intuition. In Fig. 11, the original point is the representative patterns $\mathbf{p}^1$, while the coordinate axes are the strength gradient values of the first three experimental variables (fiber contents, fiber types, mixing methods).
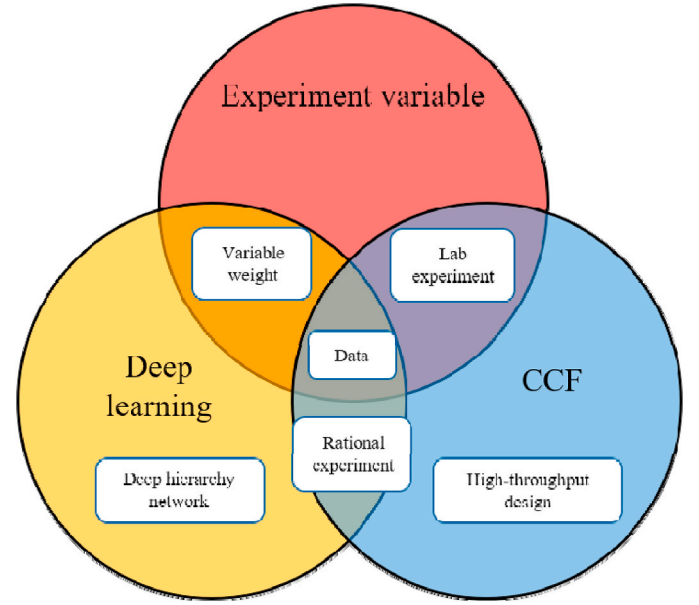
capture more intuition.

Fig. 12 summarizes how we envision the three components of our methodology, CCF, experiment variables, and deep learning, to interact. For example, one can use the gradient-based method to optimize the experimental variables. At the same time, the deep hierarchy network learns the relative importance of the design parameters, leading to more rational experiments. This is the approach we have used for CCFs. Further, one can extend this approach to fiber-reinforced silicon-based composites. The importance of detailed design based on micromechanics and fracture-mechanics still cannot be underestimated to fully understand the mechanism behind the mechanical and electrical/thermal properties that FRC demonstrates, even though this work proposed a novel method to design FRCs.

5. Conclusions

In this work, we proposed a gradient-based method for the high-throughput CCF design using deep learning. The following conclusion can be drawn:

(1) The deep hierarchy networks captured the experimental intuition from the successful-and-failed experiments, and the gradients in the deep hierarchy networks were used to represent the experimental intuition. The deep hierarchy network trained by the successful-and-failed experiments predicted the CFRC macro-properties with a 4% average error once given a set of experimental parameters. Thus, a deep hierarchy network could capture the experimental intuition from both successful and failed experiments. In addition, the quantified intuition for CFRC in a deep hierarchy network was able to be transferred into those for SFRC using a small number of the existing successful and failed experiment results.

(2) The quantified intuition and gradient-based method provided a way to design a cement-fiber-water-preparing-curing-aging system for CCFs with one or more expected properties. In the testing experiments, the method was used to compute the design parameters of CFRCs and SFRCs, which were expected to have one or more desirable macro-properties (e.g., bending strength, electrical conductivity, and thermal conductivity). The results showed that the errors between the expected and real properties of CFRCs and SFRCs were less than 8.0%. Thus, the gradient-based method had the potential for releasing the CCF property optimization from time-consuming and laborious laboratory tests.

(3) In the testing experiments, the selection ranges of the fiber properties, such as electrical conductivity, decreases with the increase in the numbers of the expected properties. This was because these experiment variables affected the CCFs' macro-properties jointly. Thus, it was not easy for a researcher to design a CCF with two or more satisfactory properties because their experimental intuition was qualitative. However, the proposed method captured and quantified the experimental intuition from the existing experiments. It overcame this problem.

(4) The normalized gradients of each experimental variable associated with $\mathbf{p}^1$, …,$\mathbf{p}^\varepsilon$ provided a statistical way to measure the contributions of an experimental variable to a CCF property. The gradient-based method based on the recorded data allowed us to quantify the experimental intuition and utilize it for the subsequent experiments.

(5) The visual explanation of the experimental intuition demonstrated that the utilization of the gradient-based method as the prior knowledge was easy for designing a CCF with the expected properties, even for someone who has little knowledge of CCFs. It had the potential to release property optimization from laboratory tests.

References

[1] Bruce J. Christensen, Tate Coverdale, Rudolf A. Olson, Steven J. Ford, Edward J. Garboczi, Hamlin M. Jennings, Thomas O. Mason, Impedance spectroscopy of hydrating cement-based materials: measurement, interpretation, and application, J. Am. Ceram. Soc. 77 (11) (1994) 2789–2804.

[2] N. Segre, I. Joekes, Use of tire rubber particles as addition to cement paste, Cement Concr. Res. 30 (9) (2000) 1421–1425.

[3] Jinping Ou, Hui Li, Structural health monitoring in mainland China: review and future trends, Struct. Health Monit. 9 (3) (2010) 219–231.

[4] Min Wu, , Björn Johannesson, Mette Geiker, A review: self-healing in cementitious materials and engineered cementitious composite as a self-healing material, Construct. Build. Mater. 28 (1) (2012) 571–583.

[5] Zongjin Li, Dong Zhang, Keru Wu, Cement-based 0-3 piezoelectric composites, J. Am. Ceram. Soc. 85 (2) (2002) 305–313.

[6] Toledo Filho, D. Romildo, Khosrow Ghavami, George L. England, Karen Scrivener, Development of vegetable fiber–mortar composites of improved durability, Cement Concr. Compos. 25 (2) (2003) 185–196.

[7] Faezeh Azhari, Nemkumar Banthia, Cement-based sensors with carbon fibers and carbon nanotubes for piezoresistive sensing, Cement Concr. Compos. 34 (7) (2012) 866–873.

[8] Anastasia Sobolkina, Viktor Mechtcherine, Vyacheslav Khavrus, Diana Maier, Mandy Mende, Manfred Ritschel, Albrecht Leonhardt, Dispersion of carbon nanotubes and its influence on the mechanical properties of the cement matrix, Cement Concr. Compos. 34 (10) (2012) 1104–1113.

[9] M. Shevlin, Practical high-throughput experimentation for chemists, ACS Med. Chem. Lett. 8 (6) (2017) 601–607.

[10] Jun Chen, Shi-cong Kou, Chi-sun Poon, Hydration and properties of nano-TiO2 blended cement composites, Cement Concr. Compos. 34 (5) (2012) 642–649.

[11] Savastano Jr., Holmer, P.G. Warden, R.S.P. Coutts, Brazilian waste fibers as reinforcement for cement-based composites, Cement Concr. Compos. 22 (5) (2000) 379–384.

[12] Biwan Xu, Zongjin Li, Paraffin/diatomite composite phase change material incorporated cement-based composite for thermal energy storage, Appl. Energy 105 (2013) 229–237.

[13] Zhu Pan, Li He, Ling Qiu, Asghar Habibnejad Korayem, Gang Li, Jun Wu Zhu, Frank Collins, Dan Li, Wen Hui Duan, Ming Chien Wang, Mechanical properties and microstructure of a graphene oxide–cement composite, Cement Concr. Compos. 58 (2015) 140–147.

[14] Jeng-Ywan Shih, Ta-Peng Chang, Tien-Chin Hsiao, Effect of nanosilica on characterization of Portland cement composite, Mater. Sci. Eng., A 424 (1-2) (2006) 266–274.

[15] M. Nehdi, Y. Djebbar, A. Khan, Neural network model for preformed-foam cellular concrete, Mater. J. 98 (5) (2001) 402–409.

[16] Tuan Nguyen, Alireza Kashani, Tuan Ngo, Stéphane Bordas, Deep neural network with high-order neuron for the prediction of foamed concrete strength, Comput. Aided Civ. Infrastruct. Eng. 34 (4) (2019) 316–332.

[17] Zhenjun Wang, Jiayu Wu, Peng Zhao, Nan Dai, Zhiwei Zhai, Ai Tao, Improving cracking resistance of cement mortar by thermo-sensitive poly N-isopropyl acrylamide (PNIPAM) gels, J. Clean. Prod. 176 (2018) 1292–1303.

[18] Zheng Tong, Jie Gao, Zhenjun Wang, Yongfeng Wei, Hui Dou, A new method for CF morphology distribution evaluation and CFRC property prediction using cascade deep learning, Construct. Build. Mater. 222 (2019) 829–838.

[19] Zheng Tong, Haoyan Guo, Jie Gao, Zhenjun Wang, A novel method for multi-scale carbon fiber distribution characterization in cement-based composites, Construct. Build. Mater. 218 (2019) 40–52.

[20] P.B. Sakthivel, A. Ravichandran, N. Alagumurthi, Modelling and prediction of flexural strength of hybrid mesh and fiber reinforced cement-based composites using Artificial Neural Network (ANN), Int. J. GEOMATE Geotech. Const. Mat. Env. 10 (2016) 1623–1635.

[21] Ahmed Ramadan Suleiman, Moncef Nehdi, Modeling self-healing of concrete using hybrid genetic algorithm–artificial neural network, Materials 10 (2) (2017) 135.

[22] L. Shi, S.T.K. Lin, Y. Lu, L. Ye, Y.X. Zhang, Artificial neural network based mechanical and electrical property prediction of engineered cementitious composites, Construct. Build. Mater. 174 (2018) 667–674.

[23] Lin Wang, Bo Yang, Ajith Abraham, Prediction of concrete strength using floating centroids method. IEEE International Conference on Systems, Man, and Cybernetics, 2013, IEEE, 2013, pp. 988–992.

[24] CECS38, 2004Technical Specification for Fiber Reinforced Concrete Structures, General Administration of Quality Supervision, Inspection and Quarantine of the People's Republic of China, Beijing, 2004.

[25] ASTM C1229-94, Standard Test Method for Determination of Glass Fiber Content in Glass Fiber Reinforced Concrete (GFRC) (Wash-Out Test), ASTM International, West Conshohocken, PA, 2015.

[26] Carlos G. Berrocal, Karla Hornbostel, Mette R. Geiker, Ingemar Löfgren, Karin Lundgren, Dimitrios G. Bekas, Electrical resistivity measurements in steel fiber reinforced cementitious materials, Cement Concr. Compos. 89 (2018) 216–229.

[27] Jie Gao, Haoyan Guo, Xiaofeng Wang, Pei Wang, Yongfeng Wei, Zhenjun Wang, Yue Huang, Bo Yang, Microwave deicing for asphalt mixture containing steel wool fibers, J. Clean. Prod. 206 (2019) 1110–1122.

[28] Jie Gao, Zhenjun Wang, Ting Zhang, Liang Zhou, Dispersion of carbon fibers in cement-based composites with different mixing methods, Construct. Build. Mater. 134 (2017) 220–227.

[29] Konsta-Gdoutos, S. Maria, Zoi S. Metaxa, Surendra P. Shah, Highly dispersed carbon nanotube reinforced cement based materials, Cement Concr. Res. 40 (7) (2010) 1052–1059.

[30] Andrzej M. Brandt, Fiber reinforced cement-based (FRC) composites after over 40 years of development in building and civil engineering, Compos. Struct. 86 (1-3) (2008) 3–9.

[31] Vasconcelos, Cristina Nader, Bárbara Nader Vasconcelos, Experiments using deep learning for dermoscopy image analysis. Pattern Recognition Letters, 2017.

[32] Vasconcelos, Cristina Nader, Bárbara Nader Vasconcelos, Increasing deep learning melanoma classification by classical and expert knowledge based image transforms, CoRR, abs 1702 (2017), 07025 1.

[33] Fernando Pacheco-Torgal, Jalali Said, Cementitious building materials reinforced with vegetable fibers: a review, Construct. Build. Mater. 25 (2) (2011) 575–581.

[34] Samuel Chuah, Zhu Pan, Jay G. Sanjayan, Chien Ming Wang, Wen Hui Duan, Nano reinforced cement and concrete composites and new perspective from graphene oxide, Construct. Build. Mater. 73 (2014) 113–124.

[35] Toledo Filho, D. Romildo, Khosrow Ghavami, George L. England, Karen Scrivener, Development of vegetable fiber–mortar composites of improved durability, Cement Concr. Compos. 25 (2) (2003) 185–196.

[36] Katrin Habel, Marco Viviani, Emmanuel Denarié, Eugen Brühwiler, Development of the mechanical properties of an ultra-high performance fiber reinforced concrete (UHPFRC), Cement Concr. Res. 36 (7) (2006) 1362–1370.

[37] Sarah L. Billington, J.K. Yoon, Cyclic response of unbonded posttensioned precast columns with ductile fiber-reinforced concrete, J. Bridge Eng. 9 (4) (2004) 353–363.

[38] Nandakumar Banthia, N. Nandakumar, Crack growth resistance of hybrid fiber reinforced cement composites, Cement Concr. Compos. 25 (1) (2003) 3–9.

[39] Ian Goodfellow, Yoshua Bengio, Aaron Courville, Deep Learning, MIT press, 2016.

[40] Yang Song, C.A. Davy, D. Troadec, X. Bourbon, Pore network of cement hydrates in a High Performance Concrete by 3D FIB/SEM—implications for macroscopic fluid transport, Cement Concr. Res. 115 (2019) 308–326.

[41] K. De Weerdt, G. Plusquellec, A. Belda Revert, M.R. Geiker, B. Lothenbach, Effect of carbonation on the pore solution of mortar, Cement Concr. Res. 118 (2019) 38–56.

[42] Raviteja Vemulapalli, Oncel Tuzel, Ming-Yu Liu, Rama Chellapa, Gaussian conditional random field network for semantic segmentation. Proceedings of the IEEE Conference on Computer Vision and Pattern Recognition, 2016, pp. 3224–3233.

[43] Zheng Tong, Dongdong Yuan, Jie Gao, Zhenjun Wang, Pavement defect detection with fully convolutional network and an uncertainty framework, Computer-Aided Civil and Infrastructure Engineering, 2020.

[44] Lin, Min, Qiang Chen, and Shuicheng Yan. "Network in network." arXiv preprint arXiv:1312.4400 (2013).

[45] Fisher Yu, Vladlen Koltun, Multi-scale context aggregation by dilated convolutions, 2015 arXiv preprint arXiv:1511.07122.

[46] David E. Rumelhart, Geoffrey E. Hinton, Ronald J. Williams, Learning representations by back-propagating errors, Cognit. Model. 5 (3) (1988) 1.

[47] Linda Argote, Organizational Learning: Creating, Retaining and Transferring Knowledge, Springer Science & Business Media, 2012.

[48] Maxime Oquab, Bottou Leon, Ivan Laptev, Josef Sivic, Learning and transferring mid-level image representations using convolutional neural networks. Proceedings of the IEEE Conference on Computer Vision and Pattern Recognition, Columbus, Ohio, 2014, pp. 1717–1724.

[49] Jie Gao, Aimin Sha, Zhenjun Wang, Liqun Hu, Di Yun, Zhuangzhuang Liu, Yue Huang, Characterization of carbon fiber distribution in cement-based composites by Computed Tomography, Construct. Build. Mater. 177 (2018) 134–147.

[50] Zheng Tong, Jie Gao, Zhenqiang Han, Zhenjun Wang, Recognition of asphalt pavement crack length using deep convolutional neural networks, Road Mater. Pavement Des. 19 (6) (2018) 1334–1349.

[51] Seyed Mohamad Moosavi, Arunraj Chidambaram, Leopold Talirz, Maciej Haranczyk, Kyriakos C. Stylianou, Berend Smit, Capturing chemical intuition in synthesis of metal-organic frameworks, Nat. Commun. 10 (1) (2019) 539.

[52] Quinn McNemar, Note on the sampling error of the difference between correlated proportions or percentages, Psychometrika 12 (2) (1947) 153–157.